ACS OMEGA

Article

Cite This: ACS Omega 2019, 4, 1007−1014

http://pubs.acs.org/journal/acsodf

Fluorescence Turn-On, Specific Detection of Cystine in Human Blood Plasma and Urine Samples by Nitrogen-Doped Carbon Quantum Dots

Gopi Kalaiyarasan,[†,‡] Chauhan Hemlata,[§] and James Joseph*[,†,‡]

[†]Electrodics and Electrocatalysis Division and [‡]Academy of Scientific and Innovative Research (AcSIR), CSIR-Central Electrochemical Research Institute (CECRI), Karaikudi 630003, India

[§]Central University of Haryana, Haryana 123031, India

Supporting Information

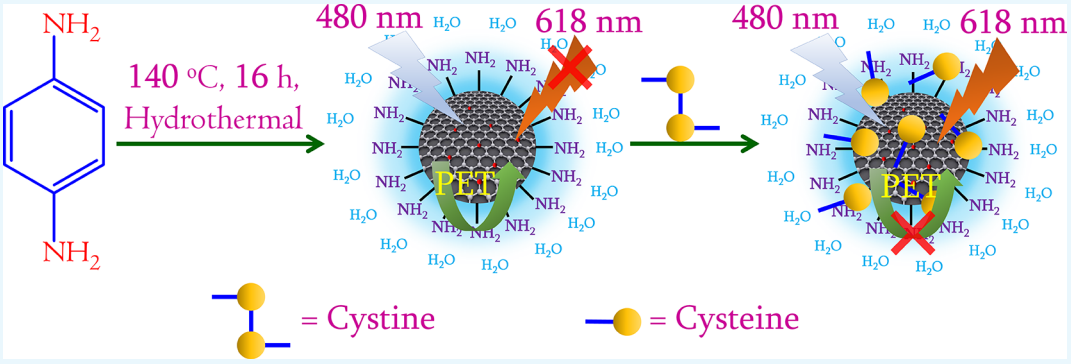

ABSTRACT: Determination of cystine in blood and urine is very important to monitor and maintain the bio metabolism, immune systems, and prevent the tissue/DNA damage from free radicals, diagnosis of cystinuria disease, cancer, and related autoimmune diseases. Among the various detection methods, fluorometric detection is simple, rapid, and sensitive to cystine using nontoxic, inexpensive, highly fluorescent, stable carbon quantum dots (CQDs). The CQDs are prepared from *p*-phenylenediamine by the hydrothermal method to get the inherent optical features of pH-dependent and excitation wavelength-independent fluorescence emission along with high aqueous stability due to pre-eminent nitrogen content. The red emission of CQDs originates from the intrinsic core that is associated with photoinduced electron transfer (PET). The turn-on fluorescence observed in presence of cystine is due to decrease in the PET by oxidation of CQDs. On the basis of this observation, we have developed an assay for the determination of cystine with a concentration range of 10 nM to 10 μM and the limit of detection is 0.4 nM. Additionally, our assay shows good recoveries (93−105%) for the spiked blood plasma and urine samples using the standard addition method.

1. INTRODUCTION

Fluorescent nanomaterials have received increased attention in recent years due to their usage in a wide range of biomedical applications, like biosensing, bioimaging, diagnosis, drug delivery, and nanomedicine.[1−6] Carbon quantum dots (CQDs) are a new class of carbon-based fluorescent materials that show high photostability against photoblinking/bleaching, high aqueous solubility, and high fluorescence quantum yield among the graphene quantum dots, graphene oxide quantum dots, and carbon nanodots.[7−9] Mostly, the fluorescence of CQDs depends on pH of the medium due to their surface functional groups like carboxylic acid and amines. Moreover, the fluorescence emission wavelength of CQDs depends on the excitation wavelength due to the existence of surface defects/states that offer the multicolor emission. If the surface defects/states are passivated by other groups like polymers or oligomers, the fluorescence originating from the electronic transition of intrinsic carbon core of the CQDs due to a quantum confinement effect leads to the excitation-independent fluorescence emission.[10] The surface passivation also helps to enhance the fluorescence intensity. Nitrogen-containing groups like amines are known to be the best passivating agents. Even though we have achieved the preparation methods to synthesize CQDs with high fluorescent quantum yield, only the blue color-emitting CQDs are often obtained and widely reported. The slight redshift in emission wavelengths was attained by the co-doping of sulfur, nitrogen, or phosphorus compared with single-element doping.[11−13] The excitation-independent green- or red-emitting CQDs are very selective and are reported in this work.

p-Phenylenediamine (*p*PD) easily undergoes polymerization reaction, and the poly-*p*-phenylenediamine (P*p*PD) is

Received: November 14, 2018
Accepted: January 2, 2019
Published: January 11, 2019

DOI: 10.1021/acsomega.8b03187
ACS Omega 2019, 4, 1007−1014

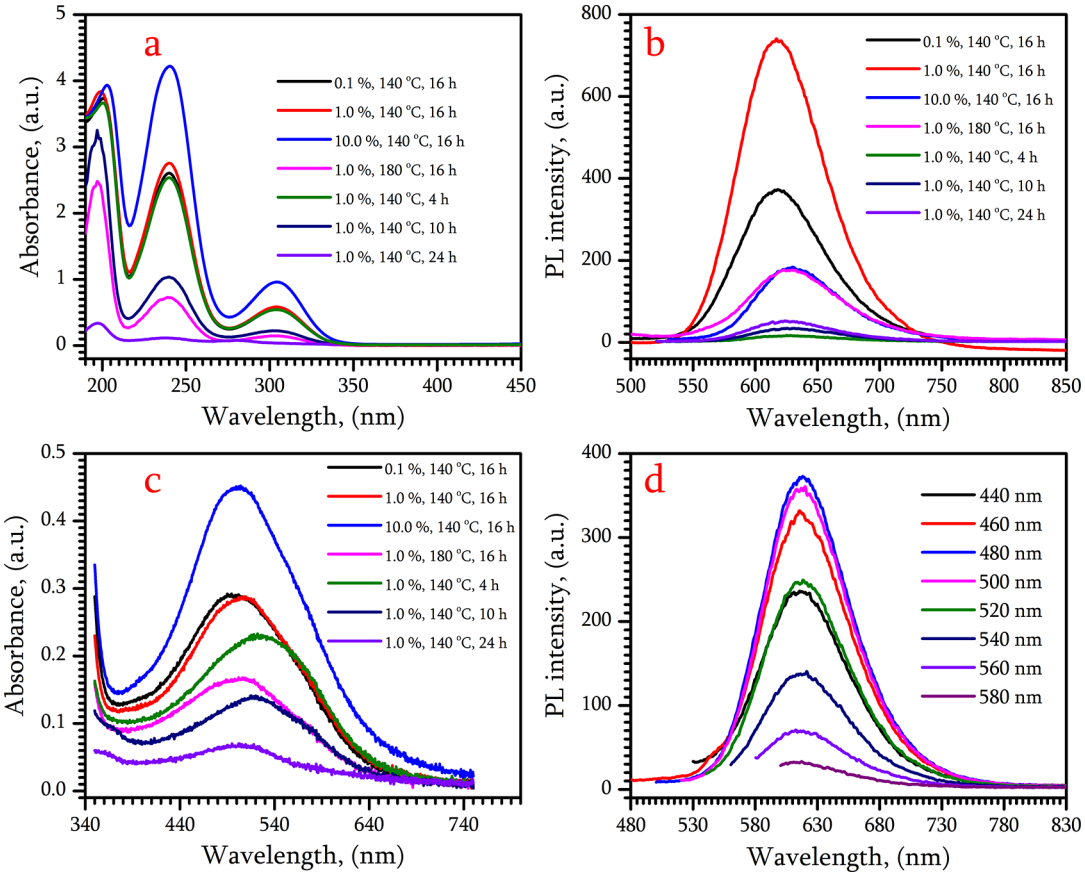

Figure 1. (a) UV−vis and (b) PL spectra of CQDs prepared from various experimental conditions (excitation wavelength is 480 nm), (c) UV−vis spectra of CQDs on the wavelength window from 350 to 750 nm, (d) PL spectra of CQDs prepared by hydrothermal treatment of 1.0% *p*PD at 140 °C for 16 h, at various excitation wavelengths ranging from 440 to 580 nm.

structurally similar to polyaniline that is widely studied and used in many fields, like energy production and storage, catalysis, and sensing.[14−18] The P*p*PD is used for the surface-passivating agent for the carbon particles to get fluorescence emission in carbon particles.[19] Jiang et al. reported the blue-, green-, and red-emitting carbon dots synthesized from *ortho*-, *meta*-, and *para*-phenylenediamine, respectively, by the solvothermal method.[20] Ding et al. reported the carbon dots derived from *p*PD along with another precursor uria by a hydrothermal method for multicolor emission by increasing oxygen moieties on their surfaces.[21] We have to synthesize CQDs from the only *p*PD by the hydrothermal method to get high fluorescence emission at a longer wavelength. Additionally, we have demonstrated their application in biosensing, especially for the selective and sensitive determination of cystine (SS-Cys). Cystine is a dimeric form of cysteine (S-Cys), generated by oxidation of cysteine. Cysteine was connected through a sulfide bond while getting oxidized. Cystine is found in many biological parts, such as skeleton, skin, connective tissues, digestive enzymes, immune system, and hair. Cystine is converted into cysteine by cystine reductase, and it is used in the synthesis of glutathione (GSH). Therefore, the increased glutathione level in liver, lungs, kidneys, and bone marrow helps in reducing the age spots (antiaging effect). Cystine is an antioxidant that prevents the DNA and tissue from free radical/reactive oxygen species attack. It is used to control cancer and similar autoimmune diseases. Also the excess concentration of cystine typically >400 mg/L in urine, leads to cystinuria, a congenital metabolic disease. Cystinuria disease can be characterized via detection of cystine stones in renal tract.[22] Very few reports are available for the detection of cystine using techniques such as chromatography,[23] iodometry,[24] spectrophotometry,[25] colorimetry,[22,26,27] and spectroflurometry.[28] For example, Lu et al. reported the detection of cystine by ascorbic acid (AA)-induced reduction of cystine in gold nanoparticle dispersion, leading to aggregation-caused color changes.[22] Wang et al reported the detection of cystine by high-performance liquid chromatography (HPLC) using dansyl chloride derivatives in reversed phase column with the use of isocratic elution.[23] These techniques have certain limitations like relatively lower sensitivity, high expense, difficult handling, toxic reagent usage, interference with other thiols, and time consumption. Therefore, selective and sensitive determination of cystine is very important in the current decade for quick screening and diagnosis of listed diseases.

Here, we have prepared red color-emitting, excitation-independent, pH-sensitive, nitrogen-doped amine-functionalized carbon quantum dots from *p*PD by a hydrothermal method for the fluorescence turn-on determination of cystine. The CQDs are clearly characterized with the help of various spectroscopic and electron microscopic studies. The optical properties of CQDs were extensively studied and distinguished and compared to those of similar CQDs available in the literature. The excitation-independent red emission in CQDs was observed without any hard synthesis procedure for the first time to the best of our knowledge. Further, the CQDs are used as a fluorescence probe to quantify the cystine in the laboratory

DOI: 10.1021/acsomega.8b03187
ACS Omega 2019, 4, 1007−1014

and real samples. The sensing mechanism is explained with the help of fluorescence/ζ-potential studies.

2. RESULTS AND DISCUSSION

2.1. Optimization and Optical Properties. Initially, three CQDs are prepared by hydrothermal treatment of *p*PD (the concentrations of *p*PD were 0.1, 1.0, and 10.0%) at 140 °C for 16 h. The UV−vis and photoluminescence (PL) spectra of those CQDs are depicted in Figure 1a,b. In Figure 1a, we can see three peaks appearing at 196, 239, and 304 nm due to $\sigma-\sigma^*$, $n-\sigma^*$, and $\pi-\pi^*$ transition of amines (C-NH_2) and aromatic carbon bonds (C═C) along with heteroatoms like nitrogen (C═N). The peak around ∼500 nm is attributed to $n-\pi^*$ transition of C═N groups that are present in CQDs prepared from 0.1% *p*PD. This peak shifted to a higher wavelength (up to 510 nm) with increasing concentration of *p*PD (Figure 1c). The increased concentration of nitrogen content leads to shifting of the wavelength to higher wavelength.[29] The higher amount of nitrogen doping enhances the fluorescence intensity and quantum yield.[30] The highest absorbance wavelength (530 nm) was observed for the CQDs prepared by a lower reaction time (4 h). Similarly, the lowest wavelength (500 nm) was observed for the CQDs prepared by a higher reaction time (24 h). Therefore, this absorbance wavelength is inversely proportional to reaction time, which means increasing the reaction time leads to a blueshift in the absorbance wavelength. The higher absorbance wavelength denotes the effective nitrogen doping on CQDs,[29] whereas as seen in the UV−vis absorbance spectra of CQDs (prepared at higher temperature, i.e., 180 °C), the wavelength is shifted to a lower wavelength (500 nm) due to lack of nitrogen doping. This observation coincided with the literature wherein it is proposing that the nitrogen doping is effective while synthesizing at a lower temperature than at higher temperature.[31,32] Therefore, the nitrogen doping is effective at a lower reaction temperature, lower reaction time, and higher concentration of precursor (*p*PD). The fluorescence spectra are recorded at different excitation wavelengths from 440 to 580 nm for CQDs (Figure 1d). The maximum emission intensity is observed at 618 nm at an excitation wavelength of 480 nm. The emission wavelength does not change with the excitation wavelength, which means the CQDs' excitation-independent emission nature may be due to uniform size, the absence of surface defects/states or those surface defects being passivated by nitrogen doping, and amine functionalization. Amines/nitrogen are known to be the best passivating groups.[7] From the results, we have selected the excitation/emission wavelengths for CQDs as 480/618 nm. PL spectra of all CQDs are shown in Figure 1b; we have observed that the CQDs that are prepared from 1.0% *p*PD at 140 °C for 16 h give maximum fluorescence emission intensity among all other CQDs. The increasing concentration of nitrogen content in CQDs leads to increasing fluorescence intensity. Additionally, the fluorescence quantum yield of all CQDs is calculated and tabulated as Table 1 with that experimental condition. From the table, we have selected CQDs that are synthesized from 1.0% *p*PD at 140 °C for 16 h under hydrothermal method on the basis of high quantum yield, for further studies.

2.2. Fourier Transform Infrared (FTIR) and X-ray Photoelectron Spectroscopy (XPS) Studies. The FTIR spectra of CQDs is depicted in Figure 2a. The characteristic stretching vibration of C═O, aromatic C═C, primary, and secondary amine groups (C−N) are observed at 1739, 1629, 1029, and 1109 cm^{-1}, respectively. It is important to note that the presence of C═O in CQDs confirms the formation of CQDs whereas *p*PD does not have the C═O vibrational frequency (Figure S1). Moreover, the C═O is present in CQDs as a six-membered ring lactone form, unlike carboxylic acid.[33] The peak at 1456 cm^{-1} is assigned to the bending vibrational frequency of N−H bond. The peaks at 2854 and 2930 cm^{-1} are assigned to C−H bond of aromatic carbon (C−C−H) and nitrogen/oxygen (N−C−H/O−C−H), respectively. The wavenumber of C═C bond in CQDs was decreased from the wavenumber of C═C of *p*PD (1637 cm^{-1}) about 10 cm^{-1} due to increasing the π-conjugation. The peak at 1260 cm^{-1} is assigned to the stretching frequency of aromatic ethers like C−O bond. Additionally, the peak at 3433 cm^{-1} is attributed to the stretching frequency of N−H of aromatic primary amines that are present on surfaces of CQDs. These functional groups are further proved with the help of XPS spectra. The XPS full survey spectrum of CQDs is plotted in Figure S2. It shows three peaks around 284 eV (82%), 400 eV (11%), and 531 eV (7%) due to C 1s, N 1s, and O 1s, respectively. As shown in Figure 2b, the C 1s peak can be deconvoluted into three peaks by Gaussian fit, at 284.6 eV (42%), 285.7 eV (36%), and 288.0 eV (4.0%). These peaks can be assigned to C−C/C═C, C−N, and C═N/C═O, respectively.[7,32] We don't find any highly oxidized carbon groups like carboxylic acid in high-resolution C 1s XPS spectrum. Additionally, as shown in Figure 2c, the N 1s peak can be deconvoluted into two peaks by Gaussian fit at 398.4 eV (4.0%) and 399.3 eV (7.0%). These peaks are assigned to pyridinic nitrogen and terminal amine groups.[7,21] As well as the O 1s peak can be deconvoluted into only one peak by Gaussian fit, which can be assigned to keto groups of CQDs possibly present on their surfaces (Figure 2d). Therefore, the synthesized material is nitrogen-doped amino-dominant carbon quantum dots. These functional groups are used to enhance the aqueous dispersibility and stability.

Table 1. Experimental Conditions for CQD Preparation and Their Quantum Yield

sr. no.	concentration of *p*PD (%)	temperature (°C)	time (h)	quantum yield (%)
1	0.1	140	16	2.8
2	1.0	140	16	3.2
3	10.0	140	16	2.3
4	1.0	180	16	2.5
5	1.0	140	4	2.4
6	1.0	140	10	2.3
7	1.0	140	24	2.4

2.3. Topological Studies. The high-resolution transmission electron microscopy (HRTEM) image of CQDs is shown in Figure 3a. The dots are uniformly dispersed and highly stable in an aqueous medium. The size of CQDs is measured from 3 to 8 nm, and the distribution curve shows the average size of dots as 5 nm (Figure 3b). At higher magnification, we have found fringes for a single dot, as shown in Figure 3c. From the fringes, we calculated the *d*-spacing and matched with the similar carbon material. The calculated *d*-spacing values are 0.203 and 0.215 nm that can be assigned to (101) and (100) planes of graphitic carbon (JCPDS: 00-001-0640). Moreover, the selected area electron diffraction (SAED) pattern of CQDs shows the *d*-spacing of 0.123 and 0.203 nm in Figure 3d. These d spacings can be

DOI: 10.1021/acsomega.8b03187
ACS Omega 2019, 4, 1007−1014

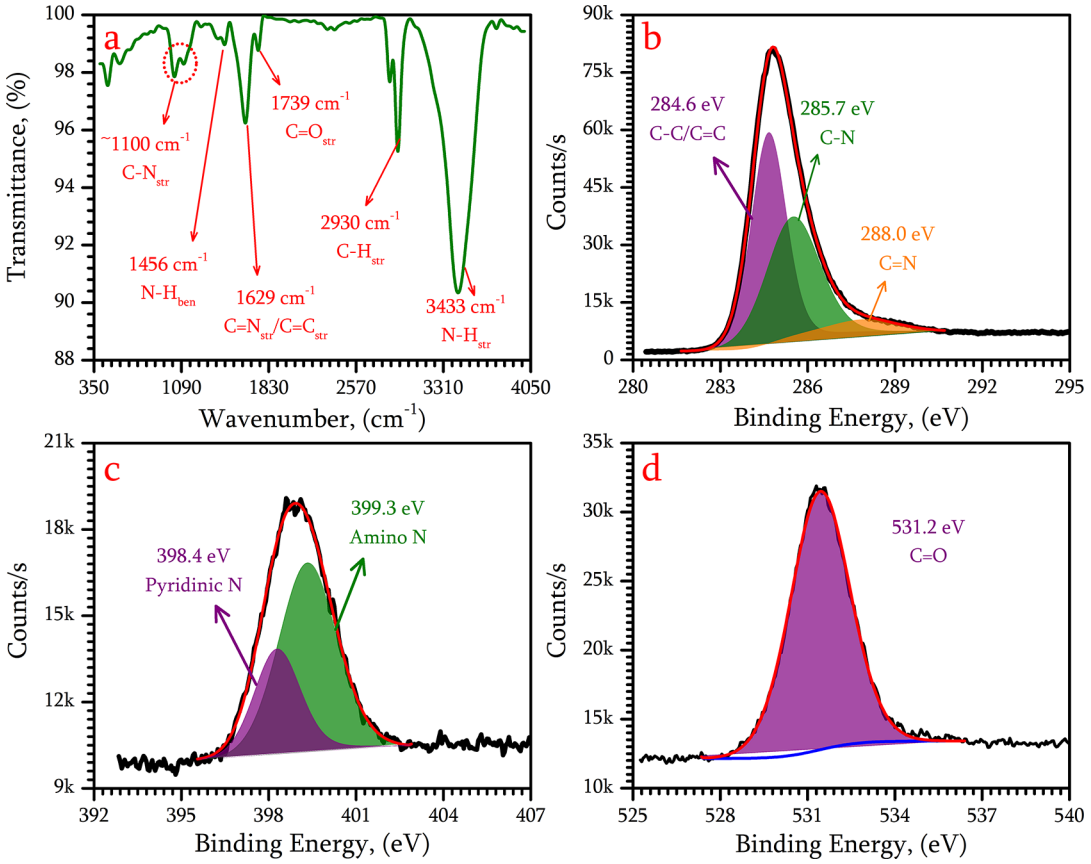

Figure 2. (a) FTIR spectrum, (b) C 1s, (c) N 1s, and (d) O 1s deconvoluted X-ray photoelectron spectra of CQDs.

assigned to (110) and (101) planes of the graphitic carbon material (JCPDS: 00-001-0640). The HRTEM images and SAED pattern established that the formed product is highly ordered graphitic carbon quantum dots.

2.4. Effect of pH Value. The fluorescence properties at acidic, neutral, and basic pH were studied. The fluorescence intensity is increased with decreasing pH, as depicted in Figure 4a. The pyridinic nitrogen at basic condition having lone pair of electrons on the outside of pyridinic ring plane. The lone pair of electrons present in the pyridinic ring will undergo nonradiative recombination via photoinduced electron transfer (PET) process.[34] Therefore, the fluorescence intensity decreased at higher pH. The pyrrolic nitrogen donates their lone pair of electrons to the pyrrolic ring that is embedded within the graphitic framework. At lower pH, there is no free loan pair electron to involve PET process. Therefore, pyridinic ring is the reason for the decreasing fluorescence intensity with increasing pH. At acidic pH, the pyridinic nitrogen gets protonated, leading to nonavailability of the free lone pair of electrons. So nonradiative recombination through PET will not be possible. Therefore, we have observed an enhancement in fluorescence at acidic pH. In the case of basic pH, we have a number of lone pair of electrons in pyridinic nitrogen and the rate of PET is very high, leading to quenching of the fluorescence. The rate of PET increased with increasing pH, leading to decrease in the fluorescence intensity. The stability of fluorescence emission was also investigated to understand the photobleaching or photoblinking effect prior to probing it. The PL spectra of CQDs at different time intervals shows negligible changes in fluorescence intensity (Figure S3). The fluorescence intensity at excitation/emission wavelength of 480/618 nm is plotted with respect to time in Figure 4b. This plot confirms that the fluorescence of CQDs is more stable over 30 min, which is sufficient for biosensing and bioimaging studies in natural samples.

2.5. Selective Determination of Cystine. Figure 5a shows the PL intensity of CQDs at excitation/emission wavelengths of 480/618 nm along with 100 μM concentrations of various biomolecules, such as ascorbic acid, uric acid (UA), dopamine (DA), cysteine, glutathione, folic acid (FA), and glucose (GOH), along with 10 μM cystine. The fluorescence intensity of CQDs with these biomolecules is decreased from that of CQDs alone. But the fluorescence intensity of CQDs with cystine is greatly increased. The mechanism for the fluorescence enhancement can be ascribed to decreasing the PET of CQDs by cystine via oxidation of CQDs. Meanwhile, cystine reduced into cysteine, which does not noticeably interfere the fluorescence of CQDs. As we know, the PET process will decrease the fluorescence due to lone pair of electrons of pyridinic nitrogen of CQDs. After adding cystine, the lone pair of electrons of pyridinic nitrogen are decreased due to oxidation of CQDs by cystine. Therefore, the amount of PET is decreased in CQDs and fluorescence intensity of CQDs is enhanced. The oxidation of CQDs is confirmed by ζ-potential measurement, which is based on the surface charge of CQDs. The ζ-potential of CQDs is found to be −45.0 mV, which shows excellent stability and increases from −45.0 to −1.5 mV after addition of 10 μM cystine (Figure 5b). It is possible that only the lone pair of electron gets eliminated or protonated (openly saying that both are oxidation reactions). The increment in ζ-potential without the addition of organic/inorganic acids is ascribed to oxidation of CQDs by cystine;

DOI: 10.1021/acsomega.8b03187
ACS Omega 2019, 4, 1007−1014

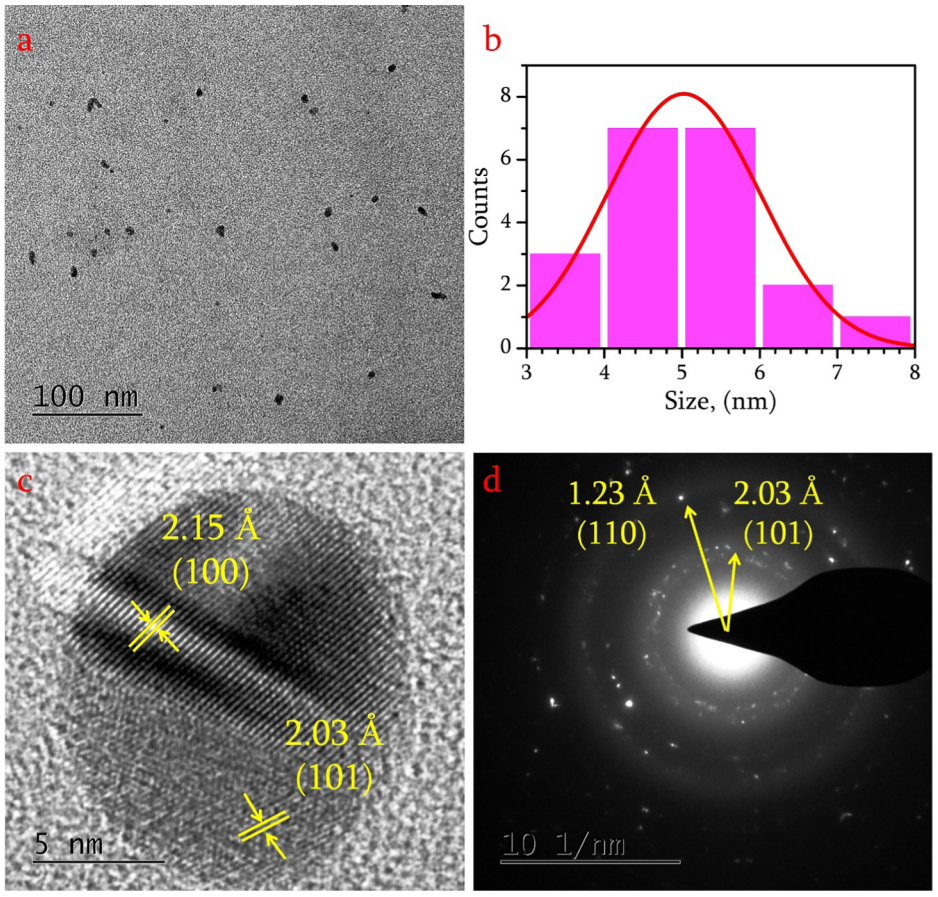

Figure 3. (a) HRTEM image of CQDs and (b) its corresponding histogram for size profile, (c) HRTEM image of CQDs at high magnification, and (d) SAED pattern of CQDs.

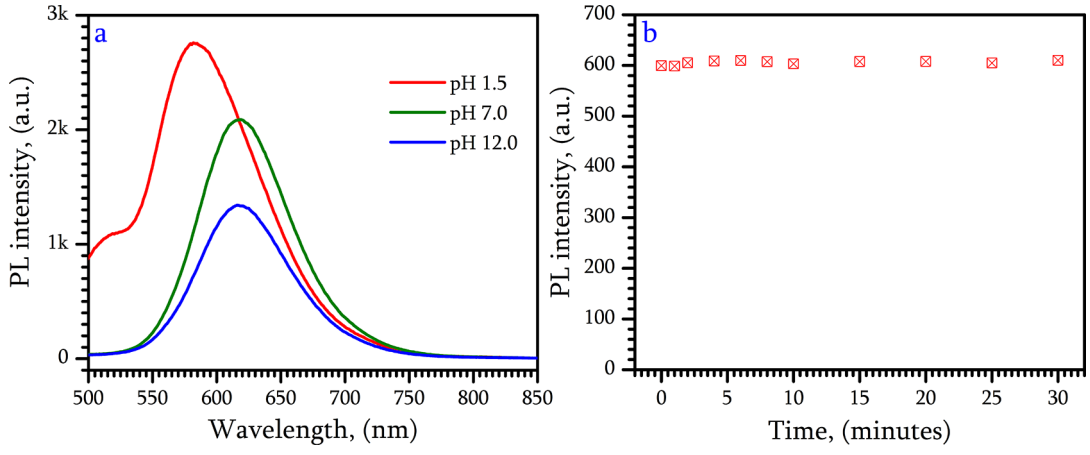

Figure 4. (a) PL spectra of CQDs at various pH, i.e., 1.5, 7.0, and 12.0 using excitation wavelength of 480 nm, (b) PL intensities of CQDs with increasing time at excitation/emission wavelength of 480/618 nm.

meanwhile, cystine gets reduced into cysteine. Therefore, the CQDs exist in oxidized form after addition of cystine. On the basis of this observation, we have added various concentrations of cystine from 10 nM to 10 μM to CQDs. The PL spectra are recorded for these samples under optimized experimental/instrumental conditions and shown in Figure 5c. The fluorescence intensity was gradually increased with increasing concentration of cystine. The corresponding calibration curve is plotted in Figure 5d. The linear range for the determination of cystine is 10 nM to 10 μM, and the limit of detection (LOD) is 0.39 nM. The sensing method, linearity, LOD, and probes in other reports are compared with our method in Table 2. From this table, it is clear, our sensing probe is the best for the selective determination of cystine. Therefore, we have studied the real sample analysis using urine and blood plasma.

2.6. Determination of Cystine in Blood and Urine Samples. We have followed the standard addition method for the determination of cystine in both blood plasma and urine samples to minimize the matrix-interfering components. We

DOI: 10.1021/acsomega.8b03187
ACS Omega 2019, 4, 1007−1014

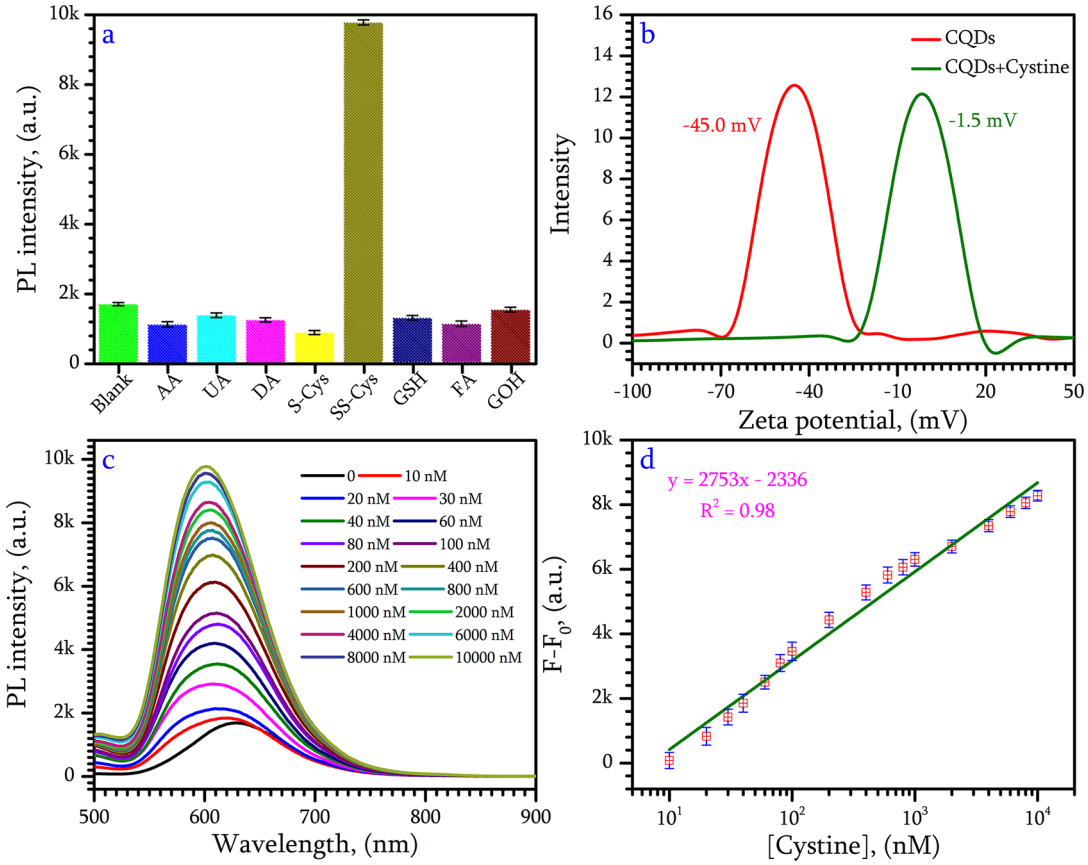

Figure 5. (a) PL intensities of CQDs alone and in presence of 100 μM concentrations of various biomolecules, such as ascorbic acid (AA), uric acid (UA), dopamine (DA), cysteine (S-Cys), glutathione (GSH), folic acid (FA), and glucose (GOH) and 10 μM cystine; (b) distribution curves of ζ-potential measurement of CQDs with/without 10 μM cystine, (c) PL spectra of CQDs before and after addition of 10 nM to 10 μM cystine (excitation wavelength of 480 nm) and (d) its PL intensity vs concentration of cystine plot for linear calibration.

Table 2. Methods of Cystine Detection for Comparison

sr. no.	methods	probe	linear range (M)	LOD (M)	ref
1	colorimetry	gold nanoparticles	$(1.0–8.0) \times 10^{-6}$	1.0×10^{-6}	22
2	HPLC	loratadine–acrylonitrile–isocratic elution	4.1×10^{-6} to 2.0×10^{-3}	1.2×10^{-6}	23
3	iodometric titration	thiols–iodine			24
4	colorimetry	oxidized dithiothreitol	8.3×10^{-6} to 8.3×10^{-5}		27
5	flow injection fluorimetry	reduction of $TlCl_3$ to TlCl	1.0×10^{-7} to5.5×10^{-6}	1.0×10^{-7}	28
6	fluorimetry	CQDs	1.0×10^{-8} to 1.0×10^{-5}	0.4×10^{-9}	this work

have chosen spiked blood plasma and urine samples as a model for the validation of our method through the standard addition method, due to nonavailability of a commercialized cystine assay kit. Human blood plasma and urine samples were collected from CSIR-CECRI health center. One micromolar and two micromolar concentrations of cystine were spiked to sample 1 and sample 2, respectively. These samples were centrifuged at RCF 8000*g* for 10 min, and the supernatant was taken for analyses after 100-fold dilution with MilliQ water to minimize the common interfering molecules. The fluorescence spectra were recorded at an excitation wavelength of 480 nm and emission intensity monitored at 618 nm of wavelength. Then, we have added a series concentration of cystine from 100 to 500 nM to the same samples. The same procedure was followed for the determination of cystine in urine samples. From the collected data of triplicate experiments, we have found the concentrations of spiked samples using the plots (Figure S4a–d) and the values are tabled as Table 3. The

Table 3. Determination of Cystine in Human Blood Plasma and Urine

		concentration of cystine (μM)			
sr. no.	sample	spiked	found	recovery (%)	RSD (%) (n = 3)
1	blood plasma	1.00	0.99	99.3	0.7
2		2.00	1.86	93.4	0.6
3	urine	5.00	5.28	105.6	0.5
4		10.00	9.96	99.6	1.2

linear regression coefficient of 0.99 with good recoveries from 93 to 105% for those experiments via standard addition method has confirmed the possibility of device fabrication for cystine detection on commercial application. However, the lone pair of electrons of pyridinic nitrogen of CQDs protonated at acidic pH condition. The fluorescence intensity is enhanced due to decreased photoinduced electron transfer

DOI: 10.1021/acsomega.8b03187
ACS Omega 2019, 4, 1007–1014

(Figure 4a). Therefore, acidic medium/contaminant should be avoided to get accurate results for cystine detection in natural samples. This limitation should be considered while making an analytical assay kit.

3. CONCLUSIONS

We have successfully synthesized red emitted carbon quantum dots from *p*-phenylenediamine by hydrothermal method. The CQDs have unique photoluminescence properties, like high quantum yield, wide excitation wavelength for monochromatic emission, pH-sensitive emission, etc. The photoinduced electron transfer-caused fluorescence quenching was found in the CQDs due to the presence of lone pair of electrons of the pyridinic nitrogen. The lone pair of electrons of pyridinic nitrogen in CQDs was decreased via oxidation of CQDs by cystine, leading to fluorescence enhancement. Using the fluorescence turn-on mechanism, we have developed an assay method for the determination of cystine in the concentration range of 10 nM to 10 μM. Additionally, the methodology was successfully used to find the concentration of spiked human blood plasma and urine samples with good recoveries (93−105%). Therefore, this method has the potential for determination of cystine in presence of major interfering compounds due to unique advantages, like high stability, inexpensiveness, rapid analysis, easy handling, etc.; thus, it can be a useful tool in bioanalytical chemistry.

4. EXPERIMENTAL SECTION

4.1. Chemicals and Reagents. *p*-Phenylenediamine (*p*PD), uric acid (UA), cysteine (S-Cys), cystine (SS-Cys), and folic acid (FA) were purchased from SRL, India. Glutathione (GSH), dopamine (DA), glucose (GOH), and vitamin B12 (VitB12) are purchased from Sigma-Aldrich. Hydrochloric acid (HCl) and ascorbic acid (AA) are purchased from MERCK. All compounds are analytical grade and used without further purification. All solutions are made in MilliQ water (18.2 MΩ cm).

4.2. Synthesis of CQDs. To synthesize CQDs, 30 mL of different concentrations of *p*PD are prepared using MilliQ water (0.1, 1.0, and 10.0%) and transferred into an autoclave (50 mL capacity). The autoclaves are kept in the furnace and maintained at different temperatures (140 and 180 °C, to understand the effect of temperature on the formation of CQDs) for different times (4, 10, 16, and 24 h, to understand the effect of reaction time on the formation of CQDs). After completion of the reaction, the autoclaves are allowed to cool at room temperature. The prepared samples are filtered using a 0.2 μm poly(tetrafluoroethylene) syringe filter, followed by 2 kDa cellulose dialysis tubing. The collected samples are initially analyzed by UV−vis and PL spectroscopy to calculate the quantum yield. The CQDs with high quantum yield were taken for further characterization and analytical studies. The quantum yield of CQDs prepared by different experimental conditions is tabulated as Table 1. The sample preparation procedure of various spectroscopic and electron microscopic analyses are explained in the Supporting Information.

4.3. Determination of Cystine and Interference Studies. Three milliliters of CQDs was taken into a quartz cuvette for the fluorescence measurement. An appropriate volume of aqueous cystine solution was added to 3 mL of CQDs to make the final concentration of cystine in a cuvette from 10 nM to 10 μM. The PL spectra recorded at 480 nm of excitation wavelength with an emission wavelength window of 500−900 nm. The fluorescence intensities at 618 nm of emission wavelength with respect to cystine concentration were taken for the calibration plot. Similarly, 100 μM concentrations of various biomolecules, such as ascorbic acid (AA), uric acid (UA), dopamine (DA), cysteine (S-Cys), glutathione (GSH), folic acid (FA), and glucose (GOH), along with 10 μM cystine (SS-Cys) were added to each 3 mL of CQDs in a quartz cuvette. The fluorescence emission intensities are directly recorded at excitation/emission wavelengths of 480/618 nm.

■ ASSOCIATED CONTENT

Supporting Information

The Supporting Information is available free of charge on the ACS Publications website at DOI: 10.1021/acsomega.8b03187.

Quantum yield calculation, experiment procedures for spectroscopic and microscopic studies, FTIR spectra of *para*-phenylenediamine (Figure S1), XPS survey spectra of CQDs (Figure S2), PL spectra of CQDs with increasing time (Figure S3), linear curve for the detection of cystine in spiked (a, b) blood plasma and (c, d) urine samples obtained by following a standard addition method (Figure S4) (PDF)

■ AUTHOR INFORMATION

Corresponding Author

*E-mail: jameskavalam@yahoo.com, jamescecri@cecri.res.in.

ORCID

Gopi Kalaiyarasan: 0000-0002-7350-4029

James Joseph: 0000-0002-4699-1466

Notes

The authors declare no competing financial interest.

■ ACKNOWLEDGMENTS

G.K. acknowledges joint CSIR-UGC, New Delhi for the award of Senior Research Fellowship.

■ REFERENCES

(1) Yao, J.; Yang, M.; Duan, Y. Chemistry, Biology, and Medicine of Fluorescent Nanomaterials and Related Systems: New Insights into Biosensing, Bioimaging, Genomics, Diagnostics, and Therapy. *Chem. Rev.* **2014**, *114*, 6130−6178.

(2) Cao, L.; Meziani, M. J.; Sahu, S.; Sun, Y.-P. Photoluminescence Properties of Graphene versus Other Carbon Nanomaterials. *Acc. Chem. Res.* **2013**, *46*, 171−180.

(3) Georgakilas, V.; Tiwari, J. N.; Kemp, K. C.; Perman, J. A.; Bourlinos, A. B.; Kim, K. S.; Zboril, R. Noncovalent Functionalization of Graphene and Graphene Oxide for Energy Materials, Biosensing, Catalytic, and Biomedical Applications. *Chem. Rev.* **2016**, *116*, 5464−5519.

(4) Lu, W.; Qin, X.; Liu, S.; Chang, G.; Zhang, Y.; Luo, Y.; Asiri, A. M.; Al-Youbi, A. O.; Sun, X. Economical, Green Synthesis of Fluorescent Carbon Nanoparticles and Their Use as Probes for Sensitive and Selective Detection of Mercury(II) Ions. *Anal. Chem.* **2012**, *84*, 5351−5357.

(5) Kalaiyarasan, G.; Narendra Kumar, A. V.; Sivakumar, C.; Joseph, J. Photoluminescence of Oligomers of Aniline-2-Sulfonic Acid Formed in the Presence of AuCl4− and Sodium Citrate: Application in the Optical Detection of Hemoglobin. *Sens. Actuators, B* **2015**, *209*, 883−888.

DOI: 10.1021/acsomega.8b03187
ACS Omega 2019, 4, 1007−1014

(6) Kalaiyarasan, G.; Anusuya, K.; Joseph, J. Melamine Dependent Fluorescence of Glutathione Protected Gold Nanoclusters and Ratiometric Quantification of Melamine in Commercial Cow Milk and Infant Formula. *Appl. Surf. Sci.* **2017**, *420*, 963−969.
(7) Kalaiyarasan, G.; Joseph, J. Determination of Vitamin B12 via PH-Dependent Quenching of the Fluorescence of Nitrogen Doped Carbon Quantum Dots. *Microchim. Acta* **2017**, *184*, 3883−3891.
(8) Lim, S. Y.; Shen, W.; Gao, Z. Carbon Quantum Dots and Their Applications. *Chem. Soc. Rev.* **2015**, *44*, 362−381.
(9) Kalaiyarasan, G.; Joseph, J. Cholesterol Derived Carbon Quantum Dots as Fluorescence Probe for the Specific Detection of Hemoglobin in Diluted Human Blood Samples. *Mater. Sci. Eng. C* **2019**, *94*, 580−586.
(10) Zhao, A.; Chen, Z.; Zhao, C.; Gao, N.; Ren, J.; Qu, X. Recent Advances in Bioapplications of C-Dots. *Carbon* **2015**, *85*, 309−327.
(11) Guo, Y.; Yang, L.; Li, W.; Wang, X.; Shang, Y.; Li, B. Carbon Dots Doped with Nitrogen and Sulfur and Loaded with Copper(II) as a "Turn-on" Fluorescent Probe for Cystein, Glutathione and Homocysteine. *Microchim. Acta* **2016**, *183*, 1409−1416.
(12) Sun, X.; Brückner, C.; Lei, Y. One-Pot and Ultrafast Synthesis of Nitrogen and Phosphorus Co-Doped Carbon Dots Possessing Bright Dual Wavelength Fluorescence Emission. *Nanoscale* **2015**, *7*, 17278−17282.
(13) Wang, W.; Lu, Y. C.; Huang, H.; Wang, A. J.; Chen, J. R.; Feng, J. J. Solvent-Free Synthesis of Sulfur- and Nitrogen-Co-Doped Fluorescent Carbon Nanoparticles from Glutathione for Highly Selective and Sensitive Detection of Mercury(II) Ions. *Sens. Actuators, B* **2014**, *202*, 741−747.
(14) Zoromba, M. S.; Abdel-Aziz, M. H.; Bassyouni, M.; Bahaitham, H.; Al-Hossainy, A. F. Poly(o-Phenylenediamine) Thin Film for Organic Solar Cell Applications. *J. Solid State Electrochem.* **2018**, *22*, 3673−3687.
(15) Zhang, Y.; Li, H.; Luo, Y.; Shi, X.; Tian, J.; Sun, X. Poly(m-Phenylenediamine) Nanospheres and Nanorods: Selective Synthesis and Their Application for Multiplex Nucleic Acid Detection. *PLoS One* **2011**, *6*, No. e20569.
(16) Smiley, R. A. Phenylene- and Toluenediamines. In *Ullmann's Encyclopedia of Industrial Chemistry*; Wiley-VCH Verlag GmbH & Co. KGaA: Weinheim, Germany, 2000; pp 25−360.
(17) Jaidev; Ramaprabhu, S. Poly(p-Phenylenediamine)/Graphene Nanocomposites for Supercapacitor Applications. *J. Mater. Chem.* **2012**, *22*, 18775−18783.
(18) Muthirulan, P.; Kannan, N.; Meenakshisundaram, M. Synthesis and Corrosion Protection Properties of Poly(o-Phenylenediamine) Nanofibers. *J. Adv. Res.* **2013**, *4*, 385−392.
(19) Craciun, A. M.; Diac, A.; Focsan, M.; Socaci, C.; Magyari, K.; Maniu, D.; Mihalache, I.; Veca, L. M.; Astilean, S.; Terec, A. Surface Passivation of Carbon Nanoparticles with: P -Phenylenediamine towards Photoluminescent Carbon Dots. *RSC Adv.* **2016**, *6*, 56944−56951.
(20) Jiang, K.; Sun, S.; Zhang, L.; Lu, Y.; Wu, A.; Cai, C.; Lin, H. Red, Green, and Blue Luminescence by Carbon Dots: Full-Color Emission Tuning and Multicolor Cellular Imaging. *Angew. Chem., Int. Ed.* **2015**, *54*, 5360−5363.
(21) Ding, H.; Yu, S.-B.; Wei, J.-S.; Xiong, H.-M. Full-Color Light-Emitting Carbon Dots with a Surface-State-Controlled Luminescence Mechanism. *ACS Nano* **2016**, *10*, 484−491.
(22) Lu, L. Q.; Gao, Q.; Song, C.; Tian, X. K.; Xu, A. W. A Novel and Environmentally Friendly Colorimetric Method for Detection of Cystine in Human Urine Using Unmodified Gold Nanoparticles. *RSC Adv.* **2014**, *4*, 27297−27300.
(23) Wang, Y.; Kang, X.-J.; Ge, W.-H.; Sun, X.-Z.; Peng, J. Simple, Rapid, and Accurate RP-HPLC Method for Determination of Cystine in Human Urine after Derivatization with Dansyl Chloride. *Chromatographia* **2007**, *65*, 527−532.
(24) Virtue, R. W.; Lewis, H. B. The Iodometric Determination of Cystine in the Urine. *J. Biol. Chem.* **1934**, *104*, 415−421.
(25) Chrastil, J. Spectrophotometric Determination of Cysteine and Cystine in Peptides and Proteins. *Analyst* **1989**, *114*, 1133−1136.
(26) Shinohara, K. The Determination of Thiol and Disulfide Compounds, with Special Reference to Cysteine and Cystine: I. Critical Study of the Color Reaction between Phospho-18-Tungstic Acid Reagent and Thiol Compounds. *J. Biol. Chem.* **1935**, *109*, 665−679.
(27) Morioka, Y.; Kobayashi, K. Colorimetric Determination of Cystine (Disulfide Bond) in Hair Using Dithiothreitol. *Biol. Pharm. Bull.* **1997**, *20*, 825−827.
(28) Ensafi, A. A.; Rezaei, B.; Nouroozi, S. Flow Injection Spectrofluorimetric Determination of Cystine and Cysteine. *J. Braz. Chem. Soc.* **2009**, *20*, 288−293.
(29) Wang, J.; Zhang, P.; Huang, C.; Liu, G.; Leung, K. C.-F.; Wáng, Y. X. J. High Performance Photoluminescent Carbon Dots for In Vitro and In Vivo Bioimaging: Effect of Nitrogen Doping Ratios. *Langmuir* **2015**, *31*, 8063−8073.
(30) Xu, M.; Xu, S.; Yang, Z.; Shu, M.; He, G.; Huang, D.; Zhang, L.; Li, L.; Cui, D.; Zhang, Y. Hydrophilic and Blue Fluorescent N-Doped Carbon Dots from Tartaric Acid and Various Alkylol Amines under Microwave Irradiation. *Nanoscale* **2015**, *7*, 15915−15923.
(31) Li, X.; Zhang, S.; Kulinich, S.; Liu, Y.; Zeng, H. Engineering Surface States of Carbon Dots to Achieve Controllable Luminescence for Solid-Luminescent Composites and Sensitive Be2+ Detection. *Sci. Rep.* **2015**, *4*, No. 4976.
(32) Qu, D.; Zheng, M.; Zhang, L.; Zhao, H.; Xie, Z.; Jing, X.; Haddad, R. E.; Fan, H.; Sun, Z. Formation Mechanism and Optimization of Highly Luminescent N-Doped Graphene Quantum Dots. *Sci. Rep.* **2015**, *4*, No. 5294.
(33) Coates, J. Interpretation of Infrared Spectra, A Practical Approach. In *Encyclopedia of Analytical Chemistry*; John Wiley & Sons, Ltd: Chichester, UK, 2006; pp 10815−10837.
(34) Hu, R.; Li, L.; Jin, W. J. Controlling Speciation of Nitrogen in Nitrogen-Doped Carbon Dots by Ferric Ion Catalysis for Enhancing Fluorescence. *Carbon* **2017**, *111*, 133−141.

DOI: 10.1021/acsomega.8b03187
ACS Omega 2019, 4, 1007−1014